

Progress Towards a New Computational Scheme for Aeroacoustics

Jeffrey P. Thomas*, Cheolwan Kim[†], and Philip L. Roe[‡]

W. M. Keck Foundation Laboratory for Computational Fluid Dynamics
 Department of Aerospace Engineering
 University of Michigan, Ann Arbor, Michigan 48109-2118

Abstract

To develop numerical schemes for aeroacoustics, numerical techniques based upon the upwind leapfrog method have been devised and tested on some model problems. Fourth-order variations of the upwind leapfrog scheme are studied and methods for applying these schemes to equations with source terms and non-constant coefficients are developed. Additionally, extensions of these upwind leapfrog ideas to the multi-dimensional advection equation and the acoustic system of equations in stationary and uniform flows are studied.

1 Introduction

Propagation of linear or weakly nonlinear waves, over distances comprising many wavelengths, is emerging as a challenging computational problem in several scientific disciplines, including electro-magnetics, elastodynamics, and aeroacoustics. The feasibility of such computations is largely governed by a parameter N identifying the number of grid points that must be used to resolve each wavelength without incurring unacceptable errors. The cost of computing any given three-dimensional phenomenon is proportional to the fourth power of N . Within the realm of finite-difference methods, many different approaches to reducing N are being studied. Compact methods [1], optimized finite difference [2], [3] and spectral methods [4] are all viable options.

In a paper presented to the 1993 AIAA CFD meeting [5] we explored the possibility of reducing N from the values around 30 that typify conventional CFD methods to values around 5-6, by employing generalized leapfrog methods [6, 7] on these problems. These are methods that employ three or more time levels in their stencil, and are constructed to be time-reversible, and hence free from dissipation, but biased in space to propagate char-

acteristic information in preferential directions. For one-dimensional wave propagation from left to right, typical stencils are shown in Figure 1 where the second figure represents the method which is biased in the “upwind” sense. Either scheme may be constructed by fitting a

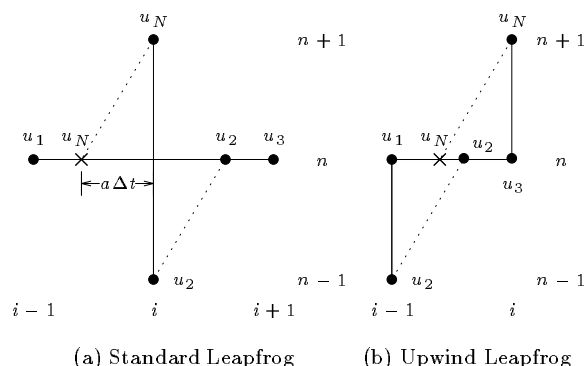


Figure 1: Second-Order Leapfrog Techniques

second-order polynomial to the data at u_1 , u_2 , and u_3 and then interpolating to $-a\Delta t$ to yield the update u_N . For propagation from right to left, this upwind stencil is mirror-imaged, and for propagation in both directions both upwind stencils are required. We developed second- and fourth-order versions in one dimension, together with a second-order version capable of being used in higher dimensions for the special case of a stationary medium, as in pure acoustics. The key to this multi-dimensional version was the use of a staggered mesh, allowing discrete bi-characteristic equations to be written that are not over-determined. This paper will describe subsequent development of these ideas.

1.1 Governing Equations

To place our efforts in context, we first set out the governing equations that we would like ultimately to be able to solve. Under the approximation that the primitive variables of density ρ , velocity components u_i , and pressure p are comprised of mean flow ($\rho_0(x_i)$, $u_{0i}(x_i)$, and $p_0(x_i)$) and transient portions ($\tilde{\rho}(x_i, t)$, $\tilde{u}_i(x_i, t)$, and

*Doctoral Candidate, Aerospace Engineering, Member AIAA

[†]Doctoral Candidate, Aerospace Engineering

[‡]Professor, Aerospace Engineering, Member AIAA

$\tilde{p}(x_i, t)$), the following linearization is made

$$\begin{aligned}\rho(x_i, t) &= \rho_0(x_i) + \varepsilon \tilde{\rho}(x_i, t) \\ u_i(x_i, t) &= u_{0i}(x_i) + \varepsilon \tilde{u}_i(x_i, t) \\ p(x_i, t) &= p_0(x_i) + \varepsilon \tilde{p}(x_i, t)\end{aligned}$$

Since ε is very small ($\mathcal{O}(10^{-5})$ for sound waves), the linearized aeroacoustic equations that govern mass, momentum and energy for the transient variables may be expressed as

$$\begin{aligned}\frac{\partial \tilde{\rho}}{\partial t} + u_{0i} \frac{\partial \tilde{\rho}}{\partial x_i} + \rho_0 \frac{\partial \tilde{u}_i}{\partial x_i} &= -\tilde{u}_i \frac{\partial \rho_0}{\partial x_i} - \tilde{\rho} \frac{\partial u_{0i}}{\partial x_i} \\ \frac{\partial \tilde{u}_i}{\partial t} + u_{0j} \frac{\partial \tilde{u}_i}{\partial x_j} + \frac{1}{\rho_0} \frac{\partial \tilde{p}}{\partial x_i} &= -\left(\tilde{u}_j + \frac{\tilde{\rho} u_{0j}}{\rho_0}\right) \frac{\partial u_{0i}}{\partial x_j} \\ \frac{\partial \tilde{s}}{\partial t} + u_{0j} \frac{\partial \tilde{s}}{\partial x_j} &= -u_{0j} \left(\frac{\tilde{\rho}}{\rho_0} \frac{\partial p_0}{\partial x_j} - \frac{\gamma \tilde{p}}{\rho_0} \frac{\partial \rho_0}{\partial x_j}\right)\end{aligned}$$

where we have defined the acoustic entropy \tilde{s} as

$$\tilde{s} = \tilde{p} - \frac{\gamma p_0}{\rho_0} \tilde{\rho} = \tilde{p} - a_0^2 \tilde{\rho}$$

and $a_0(x_i)$ is the local sound speed.

When there are no gradients in any of the mean flow quantities, the energy-entropy equation may be used to replace density in the continuity equation with pressure. In this situation, the system of equations is reduced by one, and the problem becomes one of pure acoustics, even though there may be a (uniform) mean flow.

However, when there are gradients in the mean flow, the problem is then one of aeroacoustics. The energy-entropy equation is an advective-like equation, whereas the combination of the continuity and momentum equations describe both the transport of vorticity and the propagation of acoustic waves; they are both advective and wave-like in nature. In order to treat the full aeroacoustics equations, we need to be able to devise schemes which can treat both advective and wave-like phenomena. Furthermore, we need to be able to do this for equations with non-constant coefficients and source terms.

1.2 Outline of Paper

We first note some new studies on the simple advection equation

$$u_t + au_x = 0.$$

We add to the schemes described in [5] a scheme in which the stencil is extended in time, and a ‘Hermitian’ scheme that treats the solution gradients as independent quantities to be transported. Both of these schemes are remarkably accurate, being able to maintain one percent accuracy or better with between 3 and 5 points per wavelength. This defines the standard of accuracy to which we aspire.

Generalizing the problem to include a source term creates the first problem, and we show that the apparently natural extension of the schemes can be unstable. There

is, however, a fairly simple fix. Allowing the problem to have a propagation speed and a source strength that both depend on x introduces further kinds of instabilities. These can be removed by ensuring that the equivalent equation of the scheme does not contain any anti-diffusive terms.

Then we discuss the application of these ideas to experiments in one dimension to calculate the acoustic effects of a sound source placed at the exit of a converging-diverging nozzle. We were interested to follow such calculations over very long periods of time, such that significant asymmetry of the acoustic wave envelope would develop from the weak reflections of waves from the area changes. The method as reported in [5] would eventually break down after long enough integration times, but the problem has been diagnosed, and simple modifications based on the scalar analysis have allowed both the second- and fourth-order methods to be run for several thousand time-steps with no sign of instability or accumulated error.

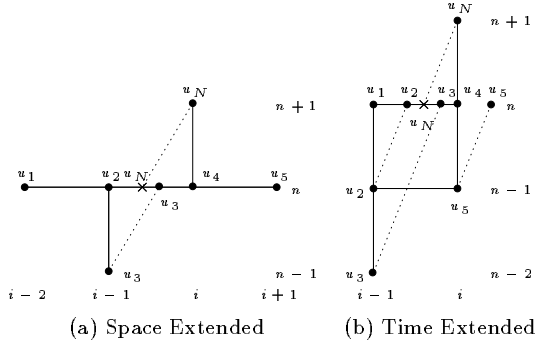
We turn then to multidimensional problems, beginning with the simplest case of scalar advection. One of the most promising approaches seems to be extending the stencils in both space and time, creating fully-discrete methods that are time-reversible and fourth-order accurate in nonuniform velocity fields. We demonstrate results for the classical test problem of a ‘Gaussian hill’ in solid-body rotation.

We report a fourth-order scheme for pure acoustics, and a second-order scheme for acoustics in the presence of a mean flow.

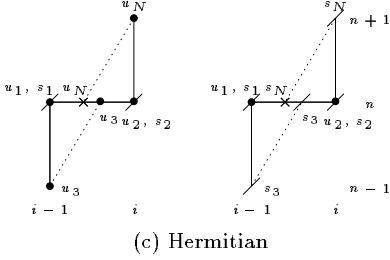
2 Fourth-Order Upwind Leapfrog Schemes for Scalar Advection

In the following, we present some methods for getting higher-order accuracy for scalar advection based on the upwind leapfrog technique. If we continue to consider the schemes for advection as interpolation routines, there are several options for gaining higher order accuracy. Since we demand zero dissipation from our schemes, their stencils must still maintain the property of time reversibility or symmetry. To get fourth-order accuracy, two additional pieces of data are necessary to fit a unique fourth-order polynomial. The two extra pieces of data may be obtained in one of three different ways. First we may stretch the stencil out in space. This is shown in figure 2a. Another way of achieving higher accuracy is to stretch the stencil in time. By keeping the data from the $n - 2$ time level one can devise another fourth scheme based on the stencil in figure 2b. Finally by updating and carrying the slopes as new variables (the *Hermitian* approach) one can devise a fourth order scheme based on the stencils in figure 2c. Even higher accuracy can of course be gained by combining these strategies.

The scheme corresponding to the extension of the



(a) Space Extended (b) Time Extended



(c) Hermitian

Figure 2: Fourth-Order Upwind Leapfrog Techniques for Scalar Advection

stencil in space is

$$u_i^{n+1} = u_{i-1}^{n-1} + \frac{(\nu+1)(2\nu-1)(\nu-2)}{2} (u_i^n - u_{i-1}^n) - \frac{\nu(\nu-1)(2\nu-1)}{6} (u_{i+1}^n - u_{i-2}^n) \quad (1)$$

and the scheme corresponding to the extension of the stencil in time is

$$u_i^{n+1} = u_{i-1}^{n-2} - \frac{3\nu-1}{2} (u_i^n - u_{i-1}^{n-1}) - \frac{(3\nu-1)(2\nu-1)}{\nu+1} (u_i^{n-1} - u_{i-1}^n). \quad (2)$$

When the Hermitian technique is employed, a total of six pieces of data are available for the polynomial interpolation $(u_i^n, u_{i-1}^n, u_{i-1}^{n-1}, u_x^n, u_{x_{i-1}}^n, u_{x_{i-1}}^{n-1})$. Using all six pieces of data yields a fifth order scheme for scalar advection. However, the resulting scheme is unstable, containing singular terms proportional to ν^{-1} and $(1-\nu)^{-1}$. A non-dissipative fourth-order scheme results from ignoring $u_{x_{i-1}}^{n-1}$ when predicting u_i^{n+1} , and ignoring u_{i-1}^{n-1} when predicting u_x^{n+1} . The scheme is, abbreviating $u_x \Delta x$ by s ,

$$u_i^{n+1} = (2\nu-1)(2\nu^2-2\nu-1)(u_i^n - u_{i-1}^n) - \nu(2\nu-1)(\nu-1)(s_i^n + s_{i-1}^n) + u_{i-1}^{n-1} \quad (3)$$

$$s_i^{n+1} = -12\nu(\nu-1)(u_i^n - u_{i-1}^n) + (6\nu^2-6\nu+1)(s_i^n + s_{i-1}^n) - s_{i-1}^{n-1} \quad (4)$$

Error		$ E = 1\%$	
Scheme	Order	$\nu = 0.25$	$\nu = 0.75$
Leapfrog	2 nd	25	17
Upwind Leapfrog	2 nd	11	6
Space Extended	4 th	4.7	3.6
Time Extended	4 th	2.1	2.0 ($\nu = 0.4$)
Hermitian	4 th	2.7	2.1

Table 1: Cells-per-Wavelength Requirements Using the Leapfrog Schemes for Scalar Advection

For each of these schemes along with the second-order standard and upwind leapfrog schemes, Figure 3 shows the phase speed error as a function of both N and ν , and Table 1 the N required for each scheme to be within one percent accuracy.

Here, we have defined this phase speed error E as

$$E\% = \left(\frac{\phi_n}{\phi_e} - 1 \right) \times 100$$

where ϕ_e , and ϕ_n represent the exact and numerical phase speeds respectively.

As can be seen from the figure, the fourth-order versions all do a much better job than their second-order relatives. In particular, the time-extended scheme shows phenomenal accuracy with only a little over two points per wavelength required to maintain at most one percent error. The Hermitian scheme has some nice properties in that a Courant number up to one may be used, and the compact stencil makes the scheme accurate and robust at boundaries. The cost, however, is that double the memory must be used.

3 Scalar Advection with a Source Term

In this section, we look at methods for using the upwind leapfrog for scalar advection with a source term

$$u_t + au_x + bu = 0$$

Straightforward application of the second-order upwind leapfrog scheme on a uniform grid leads to the scheme

$$u_{j+1}^{n+1} - u_j^{n-1} = (1-2\nu)(u_{j+1}^n - u_j^n) - b\Delta t(u_{j+1}^n + u_j^n)$$

Since this is a three-level scheme, it has two families of solutions. As usual, one family simulates the differential problem, while the other is spurious. Without any source term, both solutions are neutrally stable. Thus, if there is no strong mechanism for introducing the spurious solution, it will remain small compared with the true solution. With the source term, and the above discretization, it is easy to show that the amplification factors G_t

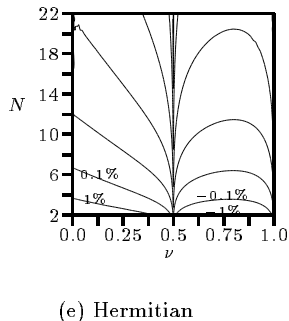
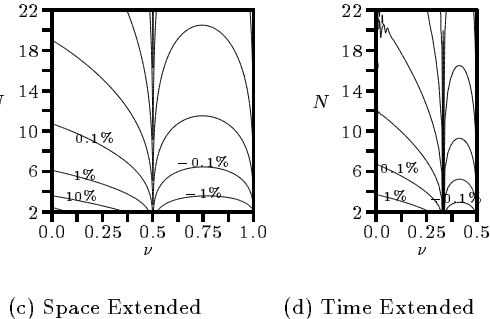
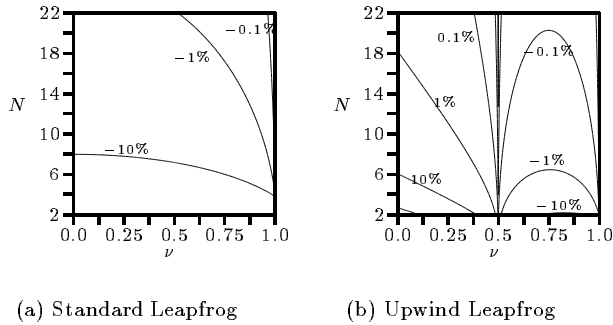


Figure 3: Phase Speed Characteristics for Various Second and Fourth-Order Leapfrog Techniques to Scalar Advection

of the true solution, and G_s of the spurious solution satisfy $G_t G_s = 1$. Thus, whenever the true solution should be decreasing ($b > 0$, $G_t < 1$), the spurious solution will grow. Even though the spurious solution may only be generated by rounding error, it will, in time, overwhelm the true solution.

In this simple case the problem can be nicely overcome by introducing the transformation

$$u = e^{-bt} v \quad \Rightarrow \quad v_t + av_x = 0$$

Applying the upwind leapfrog method to update v , and then expressing the result in terms of u , leads to the following algorithm

$$e^{b\Delta t} u_{j+1}^{n+1} - e^{-b\Delta t} u_j^{n-1} = (1 - 2\nu)(u_{j+1}^n - u_j^n).$$

By construction, we now have $G_s = G_t = e^{-b\Delta t}$, and the spurious solution never grows at the expense of the true one.

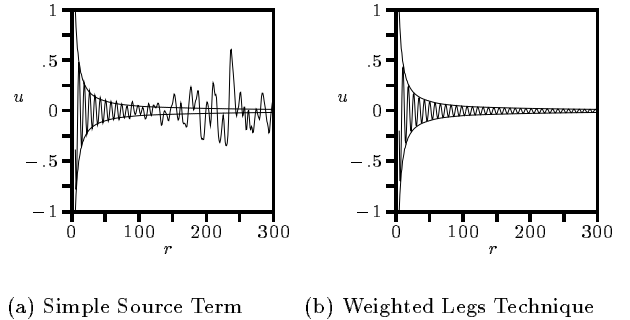


Figure 4: Two Different Variations of the Upwind Leapfrog Technique for the Spherical Wave Equation ($\Delta x = 1$, $t = 2000$, $\nu = \Delta t / \Delta r = 0.75$)

A formal generalization of this is possible by interpreting u as a vector, and a, b as matrices, with $e^{-b\Delta t}$ a matrix exponential. This generalization was successfully implemented for the nozzle problem, but it is an expensive procedure. A much more practical alternative is to abandon the idea that both amplification factors be exact, but to retain the condition that they be equal. This leads to replacing the factors $e^{\pm b\Delta t}$ by their first-order expansions $1 \pm b\Delta t$. This gives a scheme with

$$G_s = G_t = \sqrt{\frac{1 + s\Delta t}{1 - s\Delta t}} = e^{s\Delta t} + \mathcal{O}(\Delta t^3).$$

The next question is whether this local analysis provides a valid scheme for problems with non-constant coefficients; to test this we have calculated solutions to the problem

$$u_t + u_r + \frac{u}{r} = 0,$$

which represents spherically symmetric outgoing waves. Its general solution is

$$u = \frac{f(r-t)}{r}.$$

We impose sinusoidal boundary conditions at $r = 5$ and compute the solution in a domain $5 < r < 300$. With the original version of the scheme, an instability sets in after a few hundred time-steps (Figure 4), and although its amplitude never becomes catastrophic, the solution is very poor in the region $r > 100$. With the simplified modification, we can run the code on a larger domain, and the solution reaches an asymptotic state after about 500 time-steps. We've tested the scheme another 13,000 iterations and the solution envelope shows no further changes.

One way to summarize this result is that in the presence of source terms the scheme should *NOT* be reversible. In particular, the time derivative needs to be evaluated by some weighted combination of the two time differences. In the simplified scheme above, this combination would be

$$\frac{1}{2}(1 + b\Delta t) \frac{(u_{j+1}^{n+1} - u_{j+1}^n)}{\Delta t} + \frac{1}{2}(1 - b\Delta t) \frac{(u_j^n - u_j^{n-1})}{\Delta t}.$$

4 Non-Constant Coefficients and Source Term

In this section, we construct upwind leapfrog schemes applied to scalar advection with non-constant coefficients for both the advection and source terms.

$$u_t + a(x)u_x + b(x)u = 0$$

There are a multitude of ways in which to discretize the non-constant coefficients. For example, in using the upwind leapfrog scheme, we could choose the wavespeed a at x_i or x_{i-1} which we will denote as a_i or a_{i-1} . But clearly an average of the two $(a_i + a_{i-1})/2$ is what is required to achieve second-order accuracy. As for the source term, we treat it in the same manner as was described in the last section by weighting each of the time legs and then adding $(b_i + b_{i-1})(u_i^n + u_{i-1}^n)/4$. This defines the basic second-order scheme.

To create a higher-order method, we first determine the modified equation for this second-order scheme. We obtain

$$u_t + au_x + bu = -\frac{f_1u + f_2u_x + f_3u_{xx} + f_4u_{xxx}}{12a_\infty^2}\Delta x^2 + \mathcal{O}(\Delta x^4)$$

where

$$\begin{aligned} f_1 &= 2\nu^3(2b^3 - a^2b_{xx} - aa_xb_x) + 3a_\infty\nu^2(a_xb_x + ab_{xx}) \\ f_2 &= 2\nu^2(3ab^2 - aa_x^2 - a^2a_{xx} - 3a^2b_x) \\ &\quad + 3a_\infty\nu(3ab_x + aa_{xx} + a_x^2 - b^2) - 3b_xa_\infty^2 \\ f_3 &= -3a_x(-a_\infty + \nu a)(2\nu a - a_\infty) \\ f_4 &= -a(-a_\infty + \nu a)(2\nu a - a_\infty) \end{aligned}$$

Here a_∞ is a reference wave speed used to define the Courant number $\nu = a_\infty\Delta t/\Delta x$. There are no third-order error terms, so that a fourth-order scheme can be obtained by subtracting a numerical estimate of the leading error. For example, at the centroid of the stencil,

$$\begin{aligned} a &= \frac{a_i + a_{i-1}}{2} + \mathcal{O}(\Delta x^2) \\ a_x &= \frac{a_i - a_{i-1}}{\Delta x} + \mathcal{O}(\Delta x^2) \\ a_{xx} &= \frac{a_{i+1} - a_i - a_{i-1} + a_{i-2}}{\Delta x^2} + \mathcal{O}(\Delta x^2) \\ a_{xxx} &= \frac{a_{i+1} - 3a_i + 3a_{i-1} - a_{i-2}}{\Delta x^3} + \mathcal{O}(\Delta x^2), \end{aligned}$$

with similar expressions for the derivatives of b . Because the errors already contain a factor $(\Delta x)^2$ the estimates need only be, as above, second order.

We demonstrate the resulting scheme on the problem

$$u_t + \frac{u_x}{2 + \cos(2\pi x)} + \sin(2\pi x)u = 0.$$

with initial condition

$$u(x, 0) = \sin(2\pi x)$$

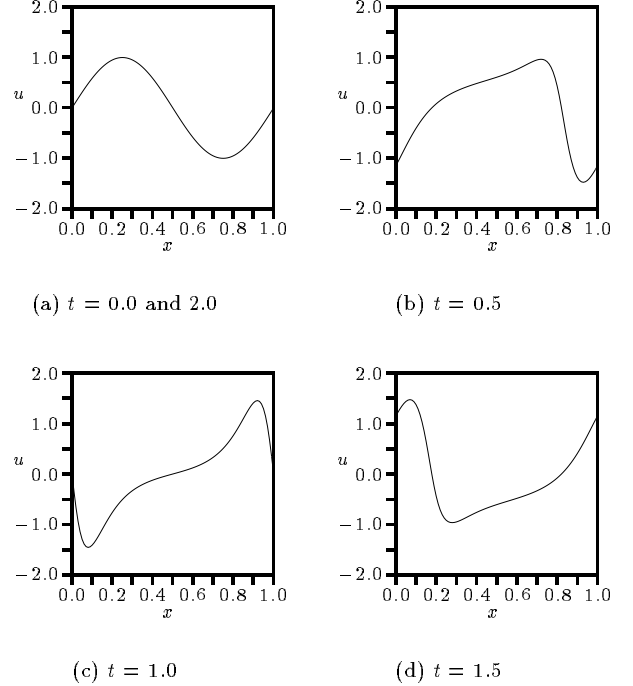


Figure 5: Model Problem Time Evolution

This equation unfortunately does not have an exact solution; however, a numerical solution that repeats with period 2.0 can be determined using a root finding technique. By using this with an extremely small tolerance, we can essentially get an exact solution. Figure 5 shows the exact solution at steps of a quarter of a cycle over the course of one period. As can be seen, the change in wavespeed and the effect of the source term cause the sine wave to become quite modified in shape over the course of a cycle.

Figure 6 shows the results of various finite-difference schemes applied to the model problem at $t = 99$, halfway through the fiftieth cycle. We choose this time since the objective of our schemes is to be able to move data on the order of 10 to 100 wavelengths, and furthermore, any errors look most noticeable at mid-cycle. In each case, a mesh of 50 cells and a Courant number of $\nu = a_\infty\Delta t/\Delta x = 1/4$ has been used. All of the three time-level schemes use the two time-level Lax-Wendroff scheme for their initial steps. In the figure, the solid and dashed lines represents the exact solution and numerical solutions respectively.

Figure 6a shows the rather poor results for the Lax-Wendroff scheme. In this version of the Lax-Wendroff scheme, the source term was simply added as $b_i u_i^n$ to the standard Lax-Wendroff scheme for scalar advection. The results show that the scheme appears to be going unstable. Better results may be obtained by a better treatment of the source term. Next, Figure 6b shows the results of the standard leapfrog scheme. Again, for this tested form of the standard leapfrog scheme, the source term was ex-

explicitly added as $b_i u_i^n$. Although the solution appears to be stable, there is a large quantity of high frequency noise. The solution was evolved for several hundred more wavelengths, yet never went unstable.

Figures 6c,d show results for upwind leapfrog scheme and the weighted time leg version of the upwind leapfrog scheme. Although, there appear to be no differences in the solutions, an examination of the L_2 norms of the solutions proves otherwise. The weighted time leg version produces slightly better results. Both schemes are stable, yet it can be seen that the dispersion error has become quite significant.

Finally, Figures 6e,f show the results for the fourth-order space extended upwind leapfrog schemes. In Figure 6e, the space extended fourth-order version of the upwind leapfrog scheme (equation 1 has been used with the wave speed simply treated as $a = (a_i + a_{i-1})/2$ and source term added as $bu = [(b_i + b_{i-1})(u_i^n + u_{i-1}^n)]/4$. As can be seen, this is an improvement over the upwind leapfrog and weighted upwind leapfrog schemes; however, this scheme does not account for the terms arising from variations in a, b and is still formally only second-order. Figure 6f finally shows how the formally fourth order technique developed above, handles this problem very well.

5 The Aeroacoustic Nozzle Problem

In this section, we address how to apply the upwind concepts studied so far to the aeroacoustic nozzle problem. The method that we reported in [5] eventually breaks down after a few hundred timesteps due to the manner in which we treated the source terms. The use of different weights for each time leg has effectively cured this problem.

Beginning with the linearized governing equations for mass, momentum and entropy for a varying area nozzle flow

$$\mathbf{u}_t + \mathbf{A}\mathbf{u}_x = \mathbf{D}\mathbf{u}$$

where (we have left off the \sim over the transient variables)

$$\mathbf{u} = \begin{bmatrix} p \\ u \\ s \end{bmatrix} \quad \mathbf{A} = \begin{bmatrix} u_o & \rho_o a_o^2 & 0 \\ 1/\rho_o & u_o & 0 \\ 0 & 0 & u_o \end{bmatrix}$$

and

$$\mathbf{D} = p_{ox} \begin{bmatrix} \frac{\gamma u_o}{\rho_o a_o^2} & \frac{-a_o^2}{u_o} & 0 \\ \frac{\rho_o a_o^2}{1} & \frac{1}{\rho_o} & \frac{1}{\rho_o a_o^2} \\ \frac{\rho_o a_o^2}{u_o(1-\gamma)} & 0 & \frac{u_o}{\rho_o a_o^2} \end{bmatrix}$$

we may create a stable upwind leapfrog scheme as follows. First, multiplying the system by left eigenvectors of \mathbf{A} leads to the characteristic form of the equations

$$\mathbf{W}_t + \mathbf{A}\mathbf{W}_x = \mathbf{S}\mathbf{W}$$

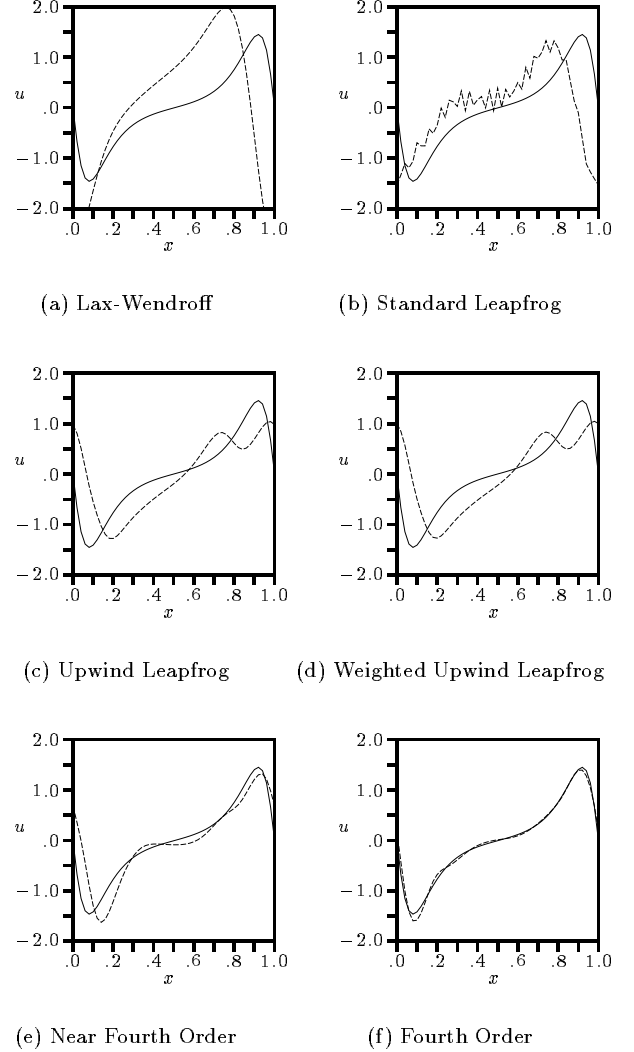


Figure 6: Various Finite-Difference Techniques for Model Problem ($t = 99$, $a_\infty = 1/2$, $\nu = a_\infty \Delta t / \Delta x = 1/4$)

where

$$\mathbf{W} = \begin{bmatrix} p + \rho_o a_o u \\ p - \rho_o a_o u \\ s \end{bmatrix} \quad \mathbf{A} = \begin{bmatrix} u_o + a_o & 0 & 0 \\ 0 & u_o - a_o & 0 \\ 0 & 0 & u_o \end{bmatrix}$$

$$\mathbf{S} = p_{ox} \begin{bmatrix} \frac{\gamma u_o^3 + a_o u_o^2 + a_o^2 u_o - a_o^3}{2\rho_o a_o^2 u_o^2} & \frac{\gamma u_o^3 + a_o u_o^2 - a_o^2 u_o + a_o^3}{2\rho_o a_o^2 u_o^2} & \frac{1}{\rho_o a_o} \\ \frac{\gamma u_o^3 - a_o u_o^2 - a_o^2 u_o - a_o^3}{2\rho_o a_o^2 u_o^2} & \frac{\gamma u_o^3 - a_o u_o^2 + a_o^2 u_o + a_o^3}{2\rho_o a_o^2 u_o^2} & \frac{-1}{\rho_o a_o} \\ \frac{u_o(1-\gamma)}{2\rho_o a_o^2} & \frac{u_o(1-\gamma)}{2\rho_o a_o^2} & \frac{u_o}{\rho_o a_o^2} \end{bmatrix}$$

Next, by introducing the transformation

$$\mathbf{W} = e^{\mathbf{S}t} \mathbf{V} \quad \Rightarrow \quad \mathbf{V}_t + \mathbf{A}\mathbf{V}_x = \mathbf{0}$$

we can generate a “weighted” time leg version of the upwind leapfrog scheme for the system of equations. If $0 < u_o < a_o$ then the discretization is

$$P_{1j} W_j|_i^{n+1} - Q_{1j} W_j|_{i-1}^{n-1} = (1 - 2\nu_1)(W_1|_i^n - W_1|_{i-1}^n)$$

$$P_{2j}W_j|_i^{n+1} - Q_{2j}W_j|_{i+1}^{n-1} = (1 + 2\nu_2)(W_2|_i^n - W_2|_{i+1}^n)$$

$$P_{3j}W_j|_i^{n+1} - Q_{3j}W_j|_{i-1}^{n-1} = (1 - 2\nu_3)(W_3|_i^n - W_3|_{i-1}^n)$$

where

$$[P] = 1 - \mathbf{S}\Delta t \approx e^{-\mathbf{S}\Delta t}$$

$$[Q] = 1 + \mathbf{S}\Delta t \approx e^{\mathbf{S}\Delta t}$$

and $\nu_i = \mathbf{A}_i\Delta t/\Delta x$. The matrices $[P]$ and $[Q]$ associated with the $(u_o + a_o)$ and u_o waves are evaluated at $i - \frac{1}{2}$ and at $i + \frac{1}{2}$ for the $(u_o - a_o)$ wave

To maintain a given noise level at the nozzle exit, the pressure is prescribed as $p_o + \epsilon \sin \omega t$. At each time step, the solution is updated by considering the Riemann problem for all pairs of consecutive grid points. Because of weak reflections from the area changes, the final grid interval usually contains an outgoing wave that gives rise to changes at the last grid point. Thus we impose, at this last grid point, a pressure change Δp sufficient to bring the new pressure to the desired level along with a velocity change $\Delta u = -\Delta p/\rho_o a_o$. Because $u_o - a_o$ is small near the throat ($M_t \approx 0.86$), we used a nonuniform grid with refinement close to the throat.

Using this technique, we are able to compute stable pressure envelopes for various mesh sizes (M) as shown in Figure 7a. The problem specification is as in [5]. These envelopes are found to remain stable even after many thousands of time integrations. Applying the techniques as described in the non-constant coefficient section, we have developed a fourth-order, and in this case, a time extended scheme which offers even better results as shown in Figure 7b. Using this fourth-order method, we are able to converge rapidly to the asymptotic envelope. Most features of aeroacoustics are present in this problem, even though confined to one dimension. The exception is that flow in a transonic throat is essentially nonlinear. Currently we are developing a uniformly-valid description of transonic acoustic waves, to avoid having to solve the full nonlinear equations in near-sonic regions.

6 Multi-dimensional Scalar Advection

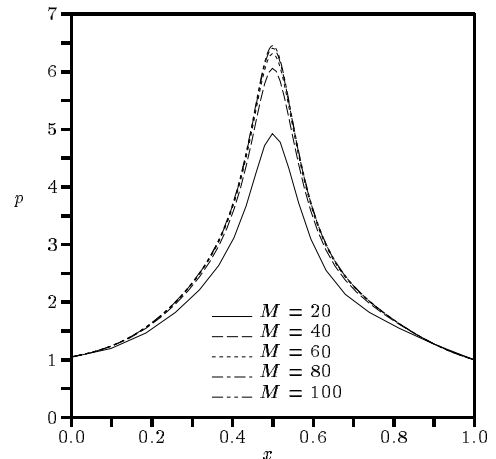
The remainder of the paper is devoted to multi-dimensional aspects. In this section, we look at higher-order upwind leapfrog scheme to handle two-dimensional scalar advection with non-constant coefficients.

$$u_t + a(x, y)u_x + b(x, y)u_y = 0$$

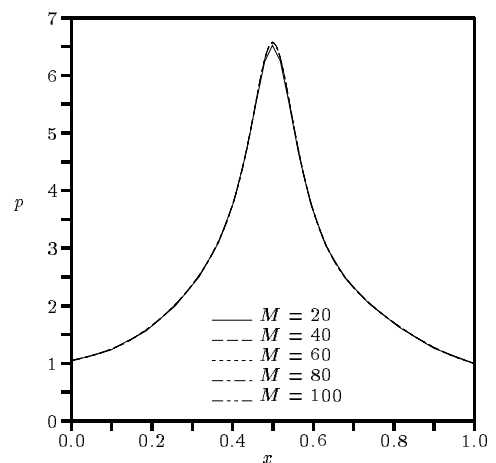
To begin with, we will look at the case where a and b are constants, such that the advection direction is given by

$$\alpha = \arctan(a/b)$$

Depending upon the advection direction, we might choose one of the four upwind leapfrog stencils shown in Figure 8. Figure 9a,b, show the dissipation and phase errors of this scheme. The solid, dashed, and thin dashed lines



(a) Second Order



(b) Fourth Order

Figure 7: Comparison of Second and Fourth Order Upwind Leapfrog Schemes for the Aeroacoustic Nozzle

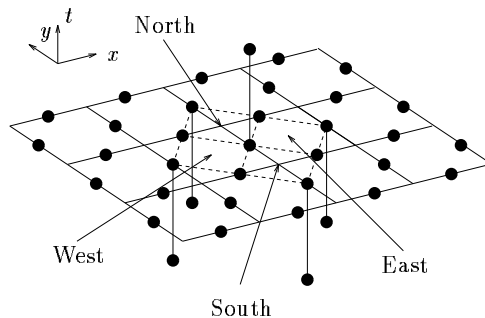
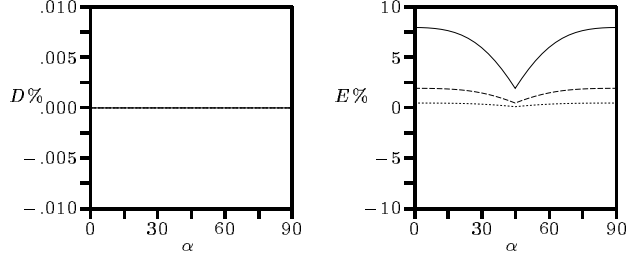
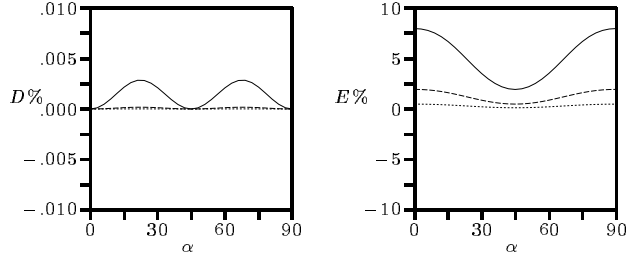


Figure 8: The Upwind Leapfrog Scheme for Two Dimensional Advection

represent trends in the cases of 4, 8, and 16 cells-per-wavelength. However, the stencil of the scheme changes abruptly when the advection direction bisects the coordinates. To avoid this we may consider blending the schemes.



(a) Amplitude Error Single (b) Phase Speed Error Single



(c) Amplitude Error Weighted (d) Phase Speed Error Weighted

Figure 9: Amplitude and Phase Speed Errors for the Single and Weighted Upwind Leapfrog Scheme for the Two Dimensional Scalar Advection Equation ($\nu_x = \nu_y = 0.25$)

If we let the capital letters N , S , E , and W denote the directions North, South, East, and West respectively, w represent weighting, and s denote scheme or stencil, then the net update may be expressed as the sum of updates from each of the stencils

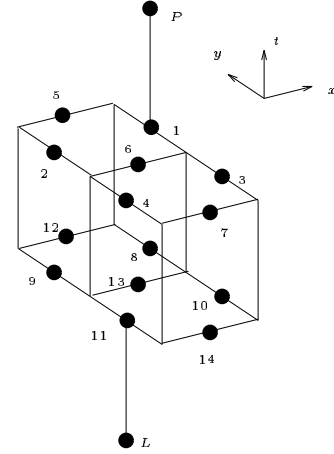
$$\text{net scheme} = w_N s_N + w_S s_S + w_E s_E + w_W s_W \quad (5)$$

One way of choosing a weighting is

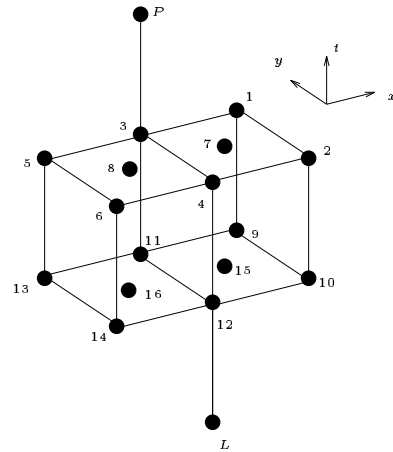
$$\begin{aligned} w_S &= \sin^2(\alpha), w_N = 0 & 0 \leq \alpha \leq \pi \\ w_S &= 0, w_N = \sin^2(\alpha) & \pi \leq \alpha \leq 2\pi \\ w_W &= 0, w_E = \cos^2(\alpha) & -\pi/2 \leq \alpha \leq \pi/2 \\ w_W &= \cos^2(\alpha), w_E = 0 & \pi/2 \leq \alpha \leq 3\pi/2 \end{aligned}$$

This leads to a slightly dissipative scheme as is shown in Figure 9c. However, we do not experience a discontinuity of slope in the phase error. The blending of two dissipation-free schemes, each with phase error $\mathcal{O}(h^p)$ can be shown to yield a scheme with the same order of phase error, but with dissipation $\mathcal{O}(h^{2p})$. The scheme will be stable if the weights are both positive. This technique for creating ‘almost non-dissipative schemes’ appears to be very useful.

To create schemes of fourth-order accuracy, we have again followed the path of subtracting from the second-order schemes numerical estimates of the errors revealed by the equivalent equation. Use of symbolic manipulation was very necessary to achieving this. We were not successful in creating a time-extended scheme in this way;



(a) Scheme 1



(b) Scheme 2

Figure 10: Quasi-Compact Time Extended Fourth-Order Upwind Leapfrog

apparently the spatial stencil must be large enough to support a steady scheme of the desired accuracy. This requirement is trivial in one dimension, but imposes limitations in higher dimensions. Purely spatial extension of the three-level schemes led to large stencils that would create problems at boundaries. We compromised by creating four-level schemes that are also somewhat extended in space, using the stencils shown in Fig.10. With the orientations as shown, the schemes are

Scheme 1

$$\begin{aligned} & Ct_1(u_p - u_1 + u_{11} - u_L) + Ct_2(u_1 - u_8 + u_4 - u_{11}) \\ & + Cx_1(u_1 - u_2 + u_{10} - u_{11}) + Cx_2(u_3 - u_4 + u_8 - u_9) \\ & + Cy_1(u_5 - u_6 + u_{13} - u_{14}) + Cy_2(u_6 - u_7 + u_{12} - u_{13}) \\ & + Cd[(u_1 - u_3 + u_2 - u_4 + u_8 - u_{10} + u_9 - u_{11}) \\ & \quad - (u_5 - u_7 + u_{12} - u_{14})] = 0 \end{aligned}$$

where

$$\begin{aligned}
Ct_1 &= \nu_x + 1, & Ct_2 &= 5\nu_x - 1, & Cd &= \nu_x \nu_y \\
Cx_1 &= 4\nu_x^2 - 2\nu_x - \nu_x \nu_y + \nu_y \\
Cx_2 &= 2\nu_x^2 + 2\nu_x + \nu_x \nu_y - \nu_y \\
Cy_1 &= \nu_y(4\nu_x - \nu_y + 1), & Cy_2 &= \nu_y(2\nu_x + \nu_y - 1)
\end{aligned}$$

Scheme 2

$$\begin{aligned}
& Ct_1(u_p - u_3 + u_{12} - u_L) + Ct_2(u_3 - u_{11} + u_4 - u_{12}) \\
& + Cx_1(u_1 - u_3 + u_{12} - u_{14}) + Cx_2(u_3 - u_5 + u_{10} - u_{12}) \\
& + Cx_3(u_7 - u_8 + u_{15} - u_{16}) + Cy_1(u_1 - u_2 + u_{13} - u_{14}) \\
& + Cy_2(u_5 - u_6 + u_9 - u_{10}) + Cy_3(u_3 - u_4 + u_{11} - u_{12}) = 0
\end{aligned}$$

where

$$\begin{aligned}
Ct_1 &= \nu_y + 1, & Ct_2 &= 5\nu_y - 1 \\
Cx_1 &= (-8\nu_x^2 + \nu_y - 6\nu_x \nu_y)/8 \\
Cx_2 &= (8\nu_x^2 - \nu_y - 6\nu_x \nu_y)/8 \\
Cx_3 &= 15\nu_x \nu_y/2 \\
Cy_1 &= (\nu_x^2 - 2\nu_x \nu_y + \nu_x + \nu_y^2 - \nu_y)/16 \\
Cy_2 &= (\nu_y^2 - \nu_y + 2\nu_x \nu_y + \nu_x^2 - \nu_x)/16 \\
Cy_3 &= (47\nu_y^2 - \nu_x^2 + \nu_y)/8
\end{aligned}$$

The stencils for these schemes appear to be the most compact possible, in that the conditions for fourth-order accuracy cannot be met with fewer points.

We have blended these two schemes together, since they are accurate at different propagation directions. Scheme 1 will be used when the advection direction is close to x-direction ($\alpha < 40^\circ$) and Scheme 2 used for the advection direction close to y-direction ($\alpha > 50^\circ$). A blend is used when $40^\circ < \alpha < 50^\circ$.

$$u_{new} = r(\alpha)u_1 + (1 - r(\alpha))u_2$$

This again introduces a slight dissipation proportional to $d\phi^2$, where $d\phi$ is the phase difference of two updated scalars. For either 4-level quasi-compact scheme, phase error is less than 0.1% with 4 grids per wavelength. Therefore, both $d\phi$ and the dissipation are very small. For example, if $d\phi$ is 0.001, the dissipation will be 10^{-6} .

To test the scheme, the following equation, representing solid-body rotation was considered

$$u_t + yu_x - xu_y = 0.$$

This equation advects the initial distribution (a Gaussian hill) along circles centered at the origin of the coordinates. Figure 11 shows the results of simulating the above equation with 4-level quasi-compact scheme on a 40×40 grid. The variation of advection speed was not considered and the scheme is only second order accurate. At $t = \pi$, the distribution starts to distort and after $t = 2\pi$, the error increases rapidly.

To achieve fourth order accuracy, the scheme was modified slightly as in Section 4, leading to the results

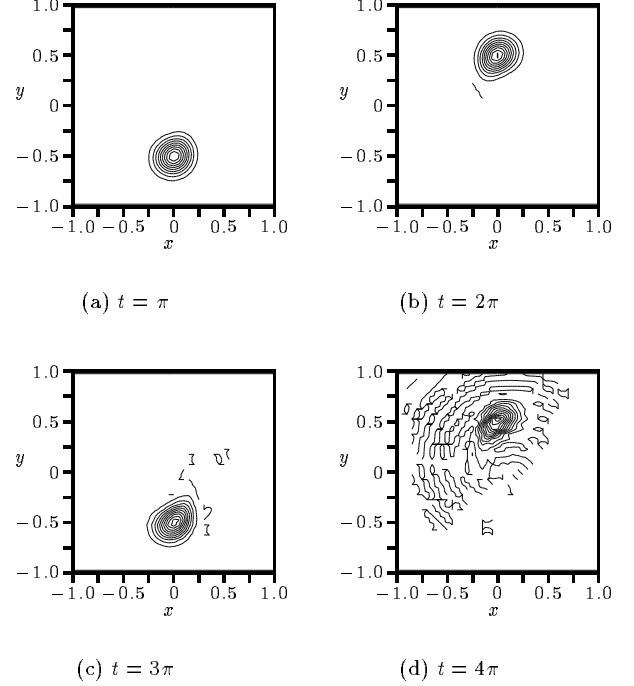


Figure 11: Second-Order Upwind Leapfrog Applied to Circular Advection of a Gaussian Hill.

shown in Figure 12. The modified scheme does not change the initial distribution shape or generate any disturbance. Because of the blending there is very slight dissipation and the peak amplitude of the disturbance decreases steadily by 1.5% over the course of six revolutions, which is consistent with the estimate given above.

7 Schemes for Acoustics in Stationary and Uniform Flows

In this section we look at some extensions of the higher-order upwind leapfrog schemes to the equations that govern acoustics in stationary or uniform flows. With given mean flow parameters (u_0, v_0, p_0, ρ_0), these equations are

$$\begin{aligned}
p_t + u_0 p_x + v_0 p_y + \rho_0 a_0^2 (u_x + v_y) &= 0 \\
u_t + u_0 u_x + v_0 u_y + (1/\rho_0) p_x &= 0 \\
v_t + u_0 v_x + v_0 v_y + (1/\rho_0) p_y &= 0
\end{aligned}$$

Multiplying these equations respectively by $1, \rho_0 a_0 \cos \alpha, \rho_0 a_0 \sin \alpha$, and adding, gives the bi-characteristic form of the equations,

$$\begin{aligned}
& (\partial_t + (u_0 + a_0 \cos \alpha) \partial_x + (v_0 + a_0 \sin \alpha) \partial_y) \times \\
& \quad \times (p + \rho_0 a_0 u \cos \alpha + \rho_0 a_0 v \sin \alpha) \\
& = \rho_0 a_0^2 (\cos \alpha \partial_y - \sin \alpha \partial_x) (v \cos \alpha - u \sin \alpha)
\end{aligned}$$

In our previous paper we devised a scheme for dealing with the case $u_0 = v_0 = 0$ and were able to create a

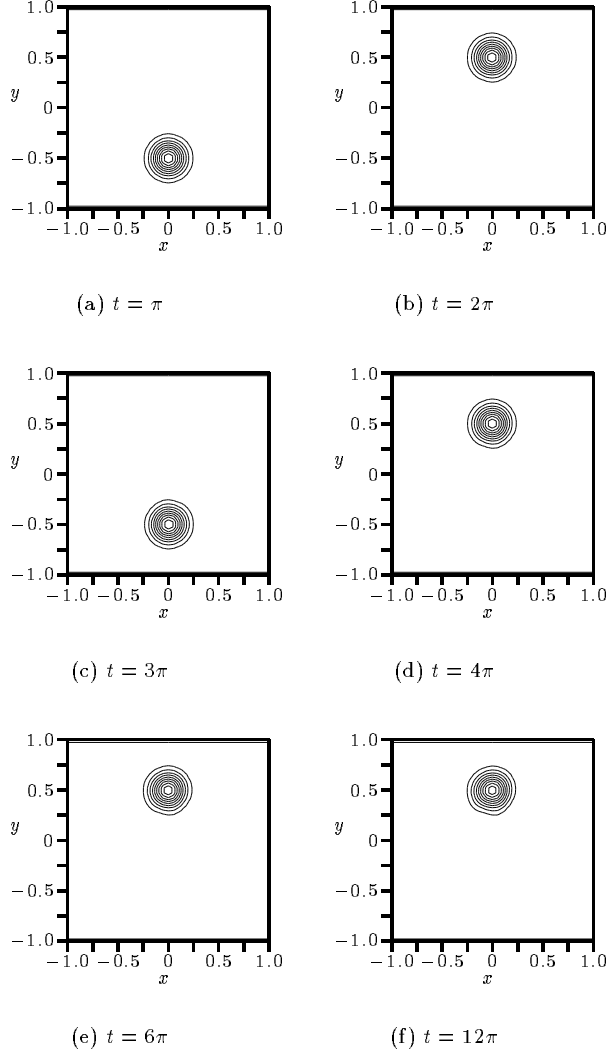


Figure 12: Fourth-Order Upwind Leapfrog Applied to Circular Advection of a Gaussian Hill.

compact, physically motivated scheme by implementing a strategy of staggered storage. In Figure 13c we show the stencil used in [5, 7] to compute the pure acoustic problem, with open circles denoting the points where p, u are stored, and black circles the points where q, v (q is an extra pressure variable) are stored. The illustrated stencil is used to discretize the wave moving in the direction $\alpha = 0$. The advantage of this staggered storage lies in the fact that we can easily discretize only those bi-characteristics for which the propagation direction is along a coordinate line. Thus, the two x -direction bi-characteristics, defined by $\alpha = 0, \pi$, are available to update two unknowns at each cell boundary where x is constant. Similar use can be made of the directions $\alpha = \pi/2, 3\pi/2$ at the boundaries where y is constant.

7.1 Dispersion Analysis

Given periodic data of the form

$$\begin{Bmatrix} p \\ u \\ v \end{Bmatrix} (x, t) = \begin{Bmatrix} P \\ U \\ V \end{Bmatrix} \exp \left[I \left(\frac{\phi t}{\Delta t} + \frac{\theta_x x}{\Delta x} + \frac{\theta_y y}{\Delta y} \right) \right]$$

the acoustic equations, within a uniform stream, will have the following exact phase speed ϕ_e relations

$$\phi_e = \begin{cases} -M_x \nu_x \theta_x - M_y \nu_y \theta_y \\ -M_x \nu_x \theta_x - M_y \nu_y \theta_y \pm \sqrt{\theta_x^2 \nu_x^2 + \theta_y^2 \nu_y^2} \end{cases}$$

where $M_x = u_0/a_0$ and $M_y = v_0/a_0$ are the coordinate Mach numbers, and $\nu_x = a_0 \Delta t / \Delta x$ and $\nu_y = a_0 \Delta t / \Delta y$ are the coordinate Courant numbers. The first quantity represents the exact phase speed for a vorticity wave, and the second two quantities represent exact phase speeds for acoustic modes. We again define E as the phase error as

$$E\% = \left(\frac{\phi_n}{\phi_e} - 1 \right) \times 100$$

where ϕ_n is the numerical phase error. In all the tests to follow, we will consider a uniform mesh, so $\nu_x = \nu_y = \nu$, and we will choose this Courant number to be 0.25. Usually it is possible to choose the Courant number larger than this, and that would improve the accuracy.

7.2 Schemes for Acoustics in Stationary Flow

We start off by examining some upwind leapfrog schemes which are applicable only for stationary acoustics ($M_x = M_y = 0$). Figure 13 shows calculated phase speed errors via Fourier/von Neumann analysis along with the computational stencils for the standard, staggered, and upwind leapfrog scheme. In each figure, the Fourier angles θ_x and θ_y are related to the number of cells-per-wavelength N and the wavefront direction α via the following relations

$$\theta_x = \frac{2\pi}{N} \cos(\alpha)$$

$$\theta_y = \frac{2\pi}{N} \sin(\alpha)$$

In each plot, we have plotted the wave direction α between 0 and 90 degrees. This was done since each of the schemes has identical properties in each quadrant on a uniform mesh. Finally, we choose 4, 8, 16 for the values of N to give an indication of order of accuracy trends.

Figure 13a shows the results for the standard leapfrog scheme. Although, very easy to construct, compared to the second-order schemes that are devised on a staggered mesh, its results are rather poor on these coarse meshes. Figure 13b shows the properties of a simple staggered leapfrog technique. This is the standard (Yee [8]) scheme used in electromagnetic simulations. Advantage is taken of the limited way that the unknowns are coupled so that only one variable is stored at each location on the mesh. Here we have drawn the stencil that would be used

to update the pressure. As can be seen there is a significant improvement over the standard leapfrog technique, however, some of the drawbacks of this scheme are that it has a Courant number limitation of $1/(2\sqrt{2}) \approx 0.35$, there are difficulties in using the scheme at computational boundaries, and the storage strategy ceases to be applicable when there is a mean flow present.

Finally, Figure 13c illustrates the properties of the upwind leapfrog scheme for stationary acoustics. The stencil in the figure represents the update for the bi-characteristic in the positive x direction. This the scheme that we presented in [5], but at that time we did not have the dispersion analysis available. This scheme has some nice properties in that it may be used at a computational boundary, and it works for a Courant number up to 0.5. Furthermore, its phase error is very symmetric about the zero phase error line, and it thus has the interesting property of having zero phase speed error for wave front angles of approximately $\alpha = 25^\circ$ and 65° for the case $\nu_x = \nu_y = 0.25$.

Figure 14 shows two methods that are based on the the Fourth-order upwind leapfrog techniques for scalar advection. In the time extended version, we have kept the stencil width to one cell which still enables us to use the scheme at computational boundaries. The scheme possesses fourth-order phase speed properties when a wave front is aligned with the mesh, however, it becomes second-order when the wave direction is oblique to the mesh. Nevertheless, it represents a big improvement over the original second-order scheme.

Figure 14b illustrates a fully fourth-order technique which we derived using the same techniques as were used to create the fourth-order scheme for non-constant coefficient scalar advection. Here, we stretched the stencil in space to obtain suitable finite difference representations to all the terms in the modified equation truncation error of the second-order upwind leapfrog scheme. These were subsequently subtracted from the upwind leapfrog discretization to obtain the resulting fourth-order method. As can be seen, the phase speed properties of this scheme are extremely good, yet there are difficulties in using this stencil at computational boundaries. This is why we do not yet have successful numerical experiments to report.

7.3 Schemes for Acoustics in Non-stationary Flows

The standard leapfrog scheme (but not the staggered version) may be used for non-stationary acoustics without any modification to its stencil since every dependent variable is stored at each mesh point. However, for the upwind leapfrog scheme, we must expand the bi-characteristic stencil in the lateral direction in order to come up with discretizations for lateral gradients (e.g. u_y , and p_y for the positive x bi-characteristic). We also found that the scheme was unstable at high wavenumbers if v_y was approximated as

$(v_{i-1/2,j+1/2}^n - v_{i-1/2,j-1/2}^n)/\Delta y$. We found that using $v_y = (v_{i-1/2,j+3/2}^n - v_{i-1/2,j-3/2}^n)/(3\Delta y)$ stabilizes the scheme.

In Figure 15 an underlying uniform flow with $M = 1/3$ is aligned at an angle of 45 degrees to the mesh, and we examine how mesh refinement effects the performance of the schemes. As can be seen, the upwind leapfrog scheme once again provides lower phase error and this error tends to be very symmetric about the zero error level. Then we use a very coarse mesh to examine the effects of Mach number (Figure 16). The upwind leapfrog scheme again shows much better phase speed properties, yet appears to have greater difficulty as the Mach number starts to increase. Perhaps we are not yet being sufficiently faithful to the physics of the problem, in which only the irrotational component of the velocity field participates in the acoustic waves.

8 Conclusions

In a continuing effort to develop efficient schemes for aeroacoustics that are based upon the upwind leapfrog scheme, we have looked at some of the main issues that need to be resolved in order to achieve this goal. These are higher accuracy, especially in the presence of source terms and variable wave speeds, and the extension to higher dimensions.

By either extending the upwind leapfrog stencil in space or time, or by updating the derivative of the dependent variable, one can derive fourth-order accurate methods. Each of these techniques is still neutrally stable, and has excellent phase properties. We have been able to make both the space and time-extended methods into the basis of more general algorithms. The Hermitian technique is harder to analyse, and as yet we do not have its multidimensional implementation.

Since the upwind leapfrog scheme is neutrally stable, one must be careful with the manner in which the source term is treated. If the source term is simply added to the discretization, instability can result. An easy fix to this problem is to weight the time legs of the stencil in an appropriate manner. Once this is accomplished, the even ordered derivative terms in the modified equation are eliminated and stability is once again achieved.

When dealing with the scalar advection equation with non-constant coefficients and source terms, one can create higher-order upwind leapfrog schemes by appropriately removing the higher-order gradient terms from the modified equation. Starting from the scheme that we developed for constant coefficient advection with a source term, we can create a fully fourth-order scheme which generates much better results than any competing second-order scheme to a simple model problem. We were able to obtain excellent results for acoustic waves in a subcritical nozzle by applying these ideas.

In two dimensions we have had some success with pure advection and with pure wave propagation. When

modelling a pure advection problem, we found that using a staggered mesh extended in space and time with a blending function to merge the updates from the coordinate aligned upwind leapfrog stencils provides a nice method. In this case the overall scheme becomes very slightly dissipative.

When modeling multi-dimensional wave-like phenomena, like acoustics, we found that by forming upwind leapfrog like discretizations to the coordinate aligned bi-characteristic equations, we can derive very efficient schemes. In addition to having better phase speed properties than the standard leapfrog scheme, the second-order upwind leapfrog scheme for stationary acoustics has the added feature that it may be used easily at computational boundaries. A time extended and fully fourth-order space extended technique offers even better results.

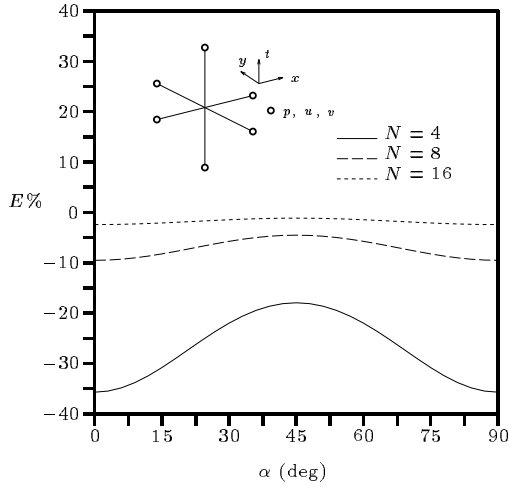
The case of non-stationary acoustics is much more difficult. So far, we have been able to derive only one upwind leapfrog scheme which is based on the stationary second order scheme. However, it still maintains much better phase speed properties than the standard leapfrog scheme. Our current work is directed toward obtaining a better synthesis of our results for the component problems.

Acknowledgments

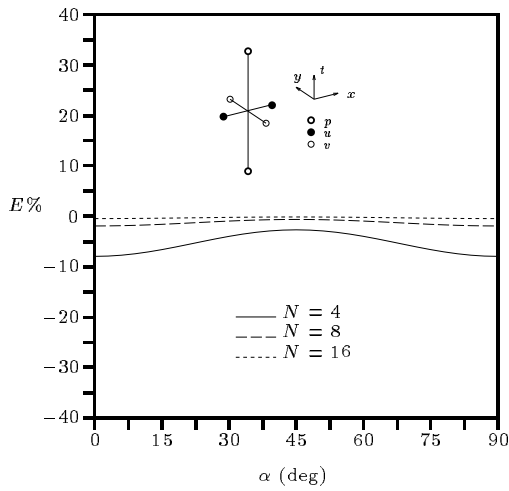
The authors would like to thank NASA for their support in the efforts that have gone into conducting this research. This work was supported under NASA contract NASA-G-NAG-1-1514.

References

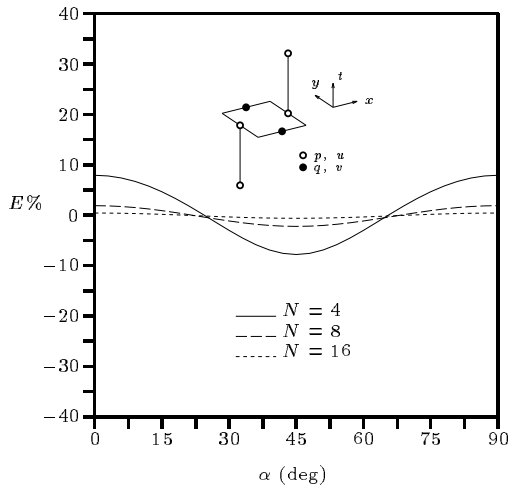
- [1] S. K. Lele. Compact finite difference schemes with spectral-like resolution. *Journal of Computational Physics*, 103:16–42, 1991.
- [2] C. K. W. Tam and J. C. Webb. Dispersion-relation-preserving finite difference schemes for computational acoustics. *Journal of Computational Physics*, 107:262–281, 1992.
- [3] D.W. Zingg, H. Lomax, and H. Jurgens. An optimized finite-difference scheme for wave propagation problems. AIAA Paper 93-0459, 1993.
- [4] D. A. Kopriva. Spectral solution of the time dependent Euler gasdynamics equations, AIAA paper DGLR/AIAA-92-02-036. In *DGLR/AIAA 14th Aeroacoustics Conference*, 1992.
- [5] J. P. Thomas and P. L. Roe. Development of nondissipation numerical schemes for computational aeroacoustics. In *AIAA 11th Computational Fluid Dynamics Conference*, 1993.
- [6] A. Iserles. Generalised leapfrog methods. *IMA Journal of Numerical Analysis*, 6, 1986.
- [7] P. L. Roe. Linear bicharacteristic schemes without dissipation. ICASE Report 94-65, 1994.
- [8] K. S. Yee. Numerical solution of initial boundary value problems involving Maxwell’s equations in isotropic media. *IEEE Trans. Antennas and Propagation*, 14, 1966.



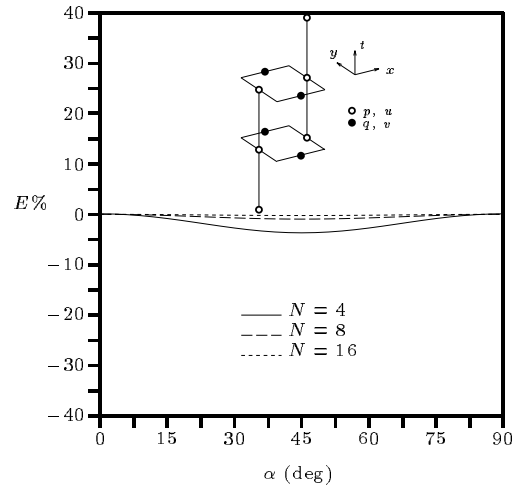
(a) Standard Leapfrog



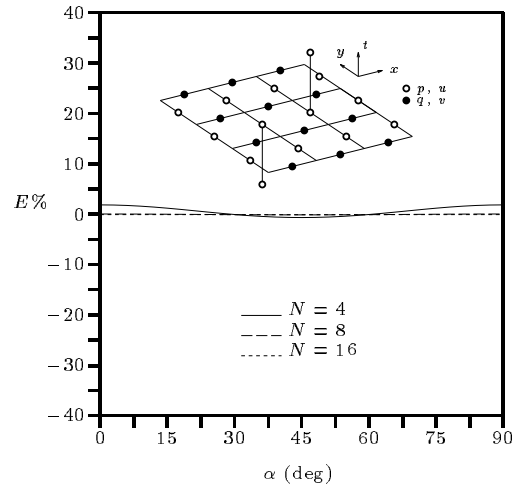
(b) Staggered Leapfrog



(c) Upwind Leapfrog



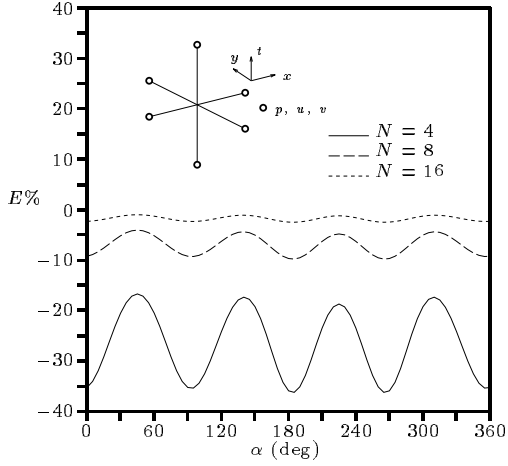
(a) Time Extended



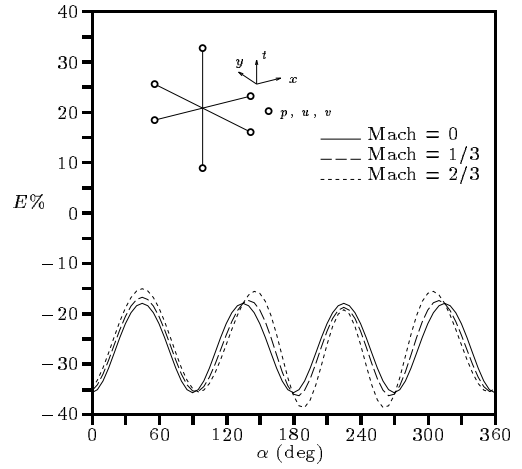
(b) Space Extended Overall Fourth-Order

Figure 14: Improved Upwind Leapfrog Schemes for Two Dimensional Stationary Acoustics

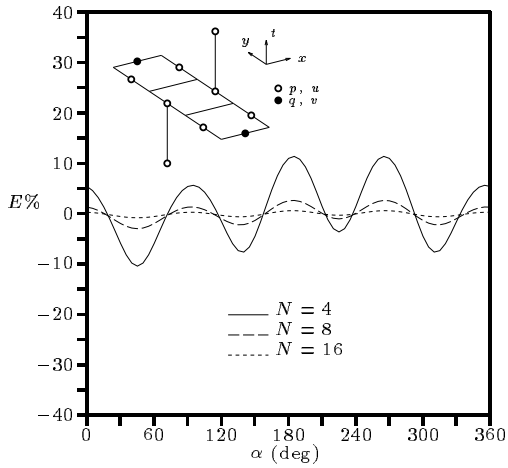
Figure 13: Leapfrog Schemes for Two Dimensional Stationary Acoustics



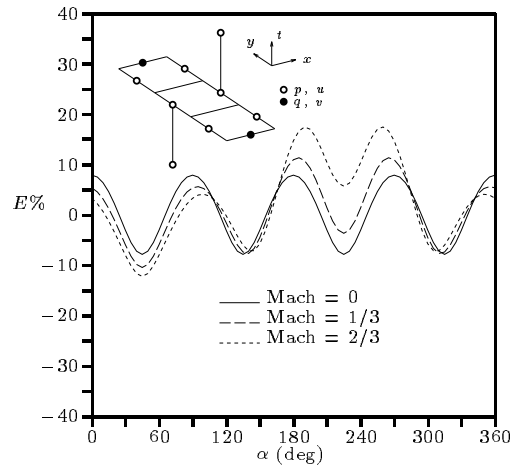
(a) Standard Leapfrog



(a) Standard Leapfrog



(b) Upwind Leapfrog



(b) Upwind Leapfrog

Figure 15: Mesh Refinement Effects for Standard and Upwind Leapfrog Schemes to the Two Dimensional Non-Stationary Acoustics $\nu_x = \nu_y = 0.25$, Mach = 1/3, Uniform Flow Direction - 45 (deg)

Figure 16: Mach Number Effects for the Standard and Upwind Leapfrog Schemes to the Two Dimensional Non-Stationary Acoustics ($\nu_x = \nu_y = 0.25$, $N = 4$)